# Internal-energy measurements of angle-resolved product $CO_2$ in catalytic CO oxidation by means of infrared chemiluminescence

Toshiro Yamanaka[a] and Tatsuo Matsushima
*Catalysis Research Center, Hokkaido University, Sapporo 001-0021, Japan*

(Received 21 November 2006; accepted 18 February 2007; published online 28 March 2007)

Measurements of both vibrational and rotational energies of product $CO_2$ in CO oxidation on palladium surfaces have been successfully performed as a function of the desorption angle by means of infrared chemiluminescence. The remarkable angle dependences of both energies indicate facile energy partitioning in repulsive desorption and provide new dimensions in the study of surface reaction dynamics as well as additional insights into the product formation site. Details of the apparatus for energy analysis of angle-resolved products are described, especially on how to pick up extremely weak infrared emission signals. © *2007 American Institute of Physics.*
[DOI: 10.1063/1.2715931]

## I. INTRODUCTION

Spatial and energy distribution measurements of emitted products are at the first stage to evaluate the potential energy surface (PES) of a chemical reaction in the gas phase.[1] Both the internal and translational energies vary when the emitted direction relative to the trajectory of the center of mass of the reaction system changes as well as when the energy or orientation of reactants is selected. In chemical reactions on solid surfaces, however, there are no reports involving successful PES analysis from the angle dependence of both internal and translational energies.[2,3] This article delivers a new angle-resolved (AR) analysis of the internal energy of emitted product $CO_2$ in the CO oxidation on palladium surfaces. Infrared chemiluminescence from the $CO_2$ is analyzed after AR procedures. The results show the remarkable desorption-angle dependences of both rotational and vibrational energies, yielding additional dimensions in the study of surface reaction dynamics. Such AR analysis could provide new structural information regarding anisotopic internal energies that cannot be obtained in the translational energy and the desorption flux.[4]

Studies of reaction dynamics on metal surfaces are still far from those in the gas phase because of the fast energy relaxation of nascent products.[5] In fact, surface spectroscopy, such as vibrational spectroscopy, diffraction, and scanning probe methods, is mostly based on the signal from nonreacting surface species, i.e., after energy dissipation. Only the desorption process yielding products with hyperthermal energy can be examined as to the energy partitioning during the reaction event.[2–4] In fact, both the internal and translational energies of such hyperthermal products have been analyzed in some exothermic desorption processes, such as $CO_2$ in the CO oxidation[4,6–12] and $H_2$ (or $D_2$) (Refs. 13–17 or $N_2$ (Refs. 18–22) in the associative desorption of H(a) or N(a). However, no PES has been examined from the angle dependences of the internal energy sensitively relatable to the product formation site. In fact, no successful angular resolved internal-energy measurements have been reported, although the site structures were already analyzed from the spatial and translational energy distributions of desorbing products.[4]

In AR product desorption analysis, surface-structural information is directly provided from the reaction event as the polar and azimuthal angle dependences of the flux or both kinetic and internal energies.[4,23–26] The internal energy would vary over these angles because the translational excitation is coupled with the rotational and vibrational ones in both adsorption and desorption processes.[13,14] The internal energy of desorbing products, however, has been analyzed in non-AR ways using infrared emission or absorption, resonance-enhanced multiphoton ionization (REMPI),[3,17] and electron beam or laser-induced fluorescence.[16,21,22] Such non-AR analysis has not provided surface-structural information because of the lack of azimuth dependence. The angle-resolved product analysis is absolutely requisite to achieve the azimuthal dependence, yielding structural information for all forms of energy and desorption flux. No structural information is provided in non-AR measurements even when large differences are found in the energy of desorbing products among surfaces with different structures. A similar structural information loss has continued in the chemical kinetics of surface reactions. A surface chemical reaction approximately shows its own structure sensitivity. The term "structure-sensitive reaction" has been used to classify the reactions with rates that have a strong dependence on the surface structures, with differences of a few orders of magnitude.[27] However, this classification has never provided information on the surface structures.

Recently, remarkable differences were found in the vibrational temperatures of desorbing product $CO_2$ in the CO oxidation between Pd(111) and Pd(110).[10] The expected anisotropy of the internal energy will be directly related to the $CO_2$ formation site structure when the energy is analyzed using AR procedures.

[a]Author to whom correspondence should be addressed; electronic mail: yama@cat.hokudai.ac.jp

 

## II. ANGLE-RESOLVED PERFORMANCE

The angle dependence of the rotational energy of emitted molecules was once examined in the photon- and electron-stimulated desorption of adsorbed NO on Pt(111),[28–31] but no significant correlation was found between the relative population of rotational states ($J$) of desorbing NO and the desorption angle, although the translational energy decreased as the desorption angle shifted from the surface normal. An ultrahigh vacuum (UHV) apparatus with a microchannel plate (MCP) detector was used in the above measurements. With the use of short laser pulses (or electron beams), the signal due to molecules directly arriving from the sample surface to the detector can be separately measured in standard time-resolved measurements because of the delayed arrival of the molecules scattered from the chamber wall.[32]

For the AR measurements of desorbing products in thermal reactions, however, the products must be selected in a definite desorption-angle range before energy analysis using a suitable slit system (collimator) and high pumping speed.[33] In the thermal reactions, the desorption of products is not pulsed. It continues for a period that is much longer than the arrival time of molecules desorbing directly from the sample surface. In fact, a one-slit system, i.e., one consisting of only a reaction chamber and an analyzer with a slit between them, cannot yield reliable angle-resolved signals. Molecules scattered from the reaction chamber wall can penetrate the analyzer and contribute significantly to the observed AR signal.

Thus, only the desorption flux and translational energy of product $CO_2$ in the CO oxidation have been analyzed in the AR way with highly sensitive mass spectrometry. The results are summarized as the product desorption is sharply collimated along the local normal to the $CO_2$ formation site, and the translational energy decreases steeply as the desorption angle shifts from the collimation angle (the maximum flux position).[4,34,35] The rotational and vibrational energies were studied only in non-AR ways by measurements of either infrared chemiluminescence from $CO_2$ or infrared absorption, as described above. No suitable REMPI route has been found for $CO_2$ molecules.[36,37]

Several difficulties are entailed in converting the infrared emission measurements into an AR form, i.e., at least two slits must be used between the sample surface and the emission collector, and high-speed pumping is requisite in the collimator housing. In the non-AR way, which was examined in a previous study, infrared emission was gathered from the product $CO_2$ passing the emission cone that was optically defined by a collector lens in the presence of reactant CO and $O_2$ at about $1\times10^{-2}$ Torr, where most of the product molecules collided with reactants before arriving at the optical cone.[10] The surviving molecules are roughly 5% or less. Nevertheless, the infrared emission from the $CO_2$ is still measurable because of the slow relaxation of excited vibrational modes of $CO_2$ (on the order of millisecond).[1,38] Eventually, the rotational modes were seriously affected by the collisions, yielding distorted internal-energy information.

In order to collect the emission before any collision, the emission cone must be set close to the surface, within at least one-tenth of the mean free path of $CO_2$, and the product molecules there are already angle resolved. Thus, the number of nascent product molecules after AR procedures is reduced to about 0.1% of that in the non-AR measurements, even at an angular resolution of about 16°. These considerations lead to ideas in which (1) the distance from a sample surface to the first slit between the reaction chamber and the collimator must be short enough to keep scattering with reactants below a tolerable level, (2) both the collimator consisting of slits and the emission collector including the optical cone must be kept under high vacuum below about $1\times10^{-5}$ Torr, and (3) the resultant weak signal must be separated from background by a complete shielding of infrared emission from surrounding walls. With high evacuation rates, the angle resolution is merely controlled by the slit size and the distances among the slits and the surface.[33]

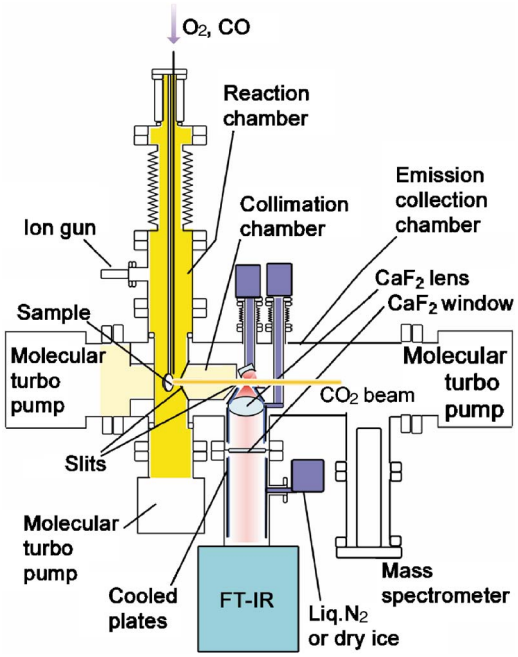


FIG. 1. (Color online) Angle-resolved emission apparatus. It consists of three chambers separately pumped by individual turbomolecular pumps, a reaction chamber, a collimator housing, and an emission collector chamber. FTIR in a separate vacuum chamber is connected to the emission collector chamber through a $CaF_2$ window. The optical cone is drawn above the $CaF_2$ lens. Three Dewars with a cooling reagent are connected separately to the optical lens, mirror and copper shields, and copper cylinder.

## III. ANGLE-RESOLVED EMISSION APPARATUS

### A. Outline of the apparatus

A schematic illustration of the apparatus designed under the above considerations is given in Fig. 1. It consists of three parts, a reaction chamber in a cylindrical shape, a collimation chamber with a slit on both ends, and an emission collector chamber. These chambers are separately pumped by individual turbomolecular pumps.

In the upper part of the reaction chamber, a palladium crystal sliced in a 10 mm diameter disk is cleaned by $Ar^+$ sputtering with a homemade ion gun and annealing in an oxygen atmosphere. After the sample crystal is cleaned, it is transferred to the center of the reaction chamber. To proceed to the CO oxidation, the sample crystal is kept at a desired

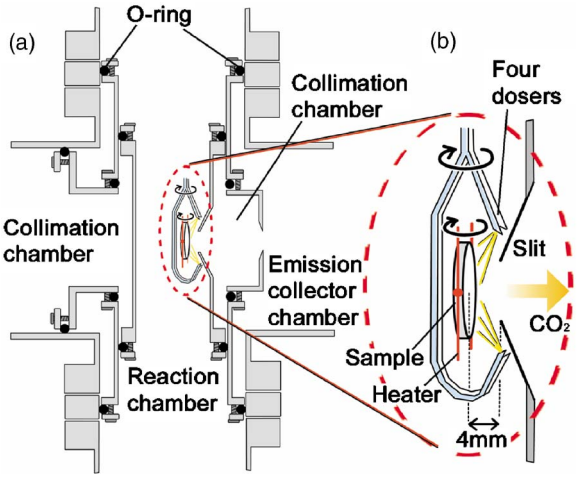


FIG. 2. (Color online) Chamber structures around a sample crystal. (a) Details of the reaction, collimation, and emission collector chambers near the sample crystal. (b) Construction of gas dosers and the first slit.

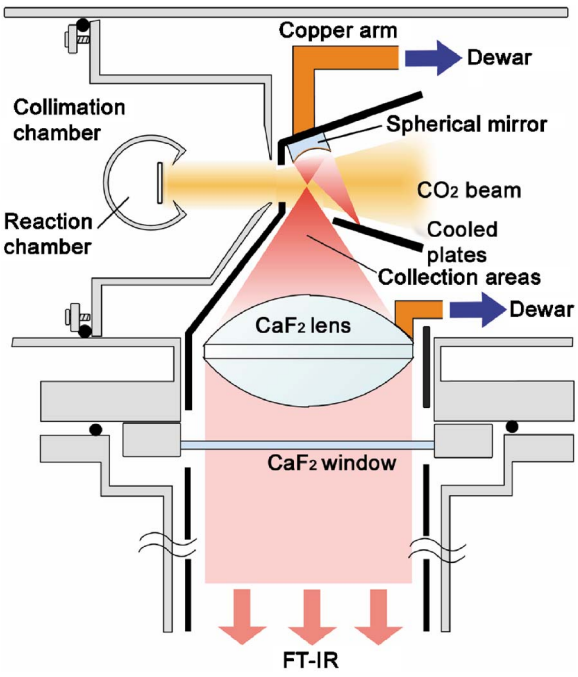


FIG. 3. (Color) Emission zone construction. A top view of the reaction, collimation, and emission collection chambers around the emission-collecting zone marked by red cones. This zone is shielded with graphite-coated copper plates cooled by either liquid nitrogen or a mixture of dry ice and methanol. The $CaF_2$ lens is connected to the second Dewar filled with ice. The FTIR spectrometer connected through a $CaF_2$ window was evacuated below $10^{-2}$ Torr. The optical path between the $CaF_2$ window and the FTIR spectrometer was shielded by a graphite-coated copper cylinder connected by the third Dewar filled by methanol–dry-ice mixture.

temperature $T_S$ by resistively heating the supporting Ta wires. The reactants $O_2$ and CO are sprayed through four gas dosers. In order to change the desorption angle, the sample crystal and dosers are rotated together without changing the geometric conditions of the gas exposure. The emitted product $CO_2$ passes the two slits and enters the emission collection chamber. In the collection chamber, infrared photons emitted in the relaxation of the antisymmetric stretch mode of product $CO_2$ $(n_1,n_2,n_3)\rightarrow(n_1,n_2,n_3-1)$ are collected by a $CaF_2$ lens and a tilted gold-coated spherical mirror and transferred to a $CaF_2$ window and then to a Fourier transform infrared (FTIR) spectrometer outside the chamber. The indices $n_1$, $n_2$, and $n_3$ are the quantum numbers of the symmetric stretch, bending, and antisymmetric stretch modes, respectively. A quadrupole mass spectrometer is also attached in the emission collector chamber to measure the $CO_2$ yield in the AR form.

The present angle resolution is only 16°, i.e., both the slits have a round shape with a diameter of 7 mm and are separated by 35 mm. The first slit is set at 4 mm from the sample surface with a 10 mm diameter. About 75% of the product $CO_2$ survives outside the first slit at a reactant pressure of $3.8\times10^{-3}$ Torr in the reaction chamber. No collision actually takes place after this position. Since only a small fraction of the scattered $CO_2$ can pass the second slit, the surviving AR-$CO_2$ reaches more than 99% of the total $CO_2$ flowing out of the second slit into the collector chamber. The resultant signal intensity is reduced to about 0.1% of that in non-AR measurements. This is primarily due to the change in the setting of the emission collector and the reduction in the reactant pressures. The signal is so weak that background infrared emission must be minimized by cooling a graphite-coated copper shield surrounding the collection area, including the optics. Thus, data collection takes about a week for a single emission spectrum. To accurately analyze this very weak chemiluminescence spectra, the signal intensities were treated as complex numbers, and the contribution from the background emission from the FTIR spectrometer itself with an unknown phase was eliminated. Details of each part are described in the following sections.

### B. Structures of the three chambers

The detailed structures of the three chambers are shown in Fig. 2. These chambers consist of several replaceable parts for easy modifications. For example, the size of both slits and their distance can be easily changed. It is also possible to eliminate one of them for the examination of each chamber. To obtain sufficient sealing with an UHV level among the three chambers, Viton O rings were inserted between connected parts. The baking of apparatus is possible to 423–473 K depending on the material of the O rings.

To keep the mean free path of the product $CO_2$ long enough, the pressures of the collimation and emission collector chambers were kept below $1\times10^{-5}$ and $1\times10^{-7}$ Torr, respectively, with high-speed pumping. On the other hand, rapid pumping is less important in the reaction chamber because of the reactant pressure of around $3\times10^{-3}$ Torr. Thus, the collimation chamber and emission collection chambers are separately pumped by large turbomolecular pumps (450 l/s) directly attached to each chamber via a conflat flange (203 mm in diameter), while the reaction chamber is pumped by a small turbomolecular pump (70 l/s) directly attached to this chamber via a conflat flange (114 mm in diameter).

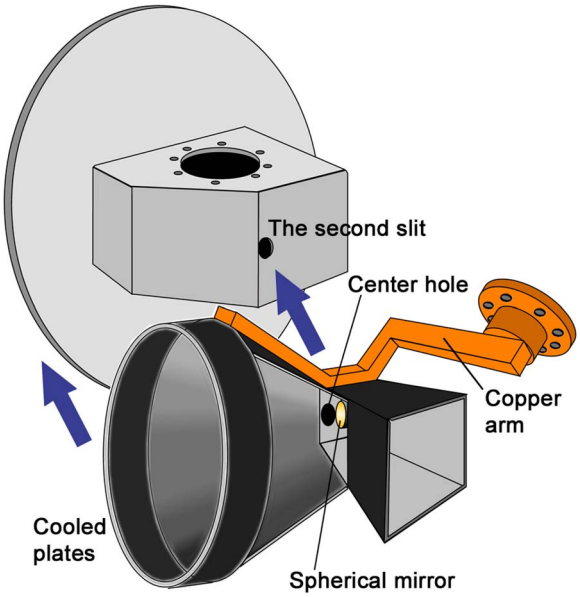


FIG. 4. (Color online) Three-dimensional illustration of the collimation chamber (upper part) and graphite-coated copper plates (dark box and cone). These plates are attached to the copper arm. The copper plate is set at a position close to the collimation chamber (the arrows) so that the center hole on it is only 0.5 mm from the second slit without touching the chamber.

### C. Structures of dosers and the first slit

In the present measurements, the intensity of infrared emission from angle-resolved $CO_2$ is very weak. Therefore, the pressures of reactant gases are increased to a certain level so that the resultant mean free path of product $CO_2$ is long enough to keep nascent product $CO_2$ free from collisions with reactants. Thus, the dosers and the first slit were designed so that the distance between the sample surface and the first slit would be as short as possible. After $CO_2$ passes the first slit, the mean free path of $CO_2$ in the collimation chamber is long enough to prevent any collisions.

The structures of the dosers and the first slit are shown in Fig. 2(b). To reduce the distance between the sample surface and the first slit, four dosers, each with a 100 $\mu$m diameter pinhole at the top, are placed close to the surface. Each doser sprays either $O_2$ or CO from the opposite grazing direction. Thus, a uniform exposure of the reactants on the surface is obtained. The shape of the first slit is conical, and two Ta wires for annealing of the sample are parallel to the rotation axis of the sample and dosers. In this situation, the distance between the sample and the first slit can be reduced to 4 mm at all necessary desorption angles. About 75% of the product $CO_2$ can enter the collimation chamber without being scattered with other molecules when the pressure in the reaction chamber is $3.7\times10^{-3}$ Torr, i.e., when a gas dosing rate is $4.5\times10^{17}$ molecules/cm$^2$ s.

### D. Detection of weak chemiluminescence and reduction of background emission

Infrared emission from product $CO_2$ is collected and transferred to a FTIR spectrometer using a $CaF_2$ lens (80 mm in diameter and focal length of 70 mm) and a gold-coated spherical mirror (10 mm in diameter and 10 mm radius of the spherical surface). Because of the very weak signals, it is necessary to reduce the background infrared emission from the chamber walls. This was accomplished by a complete shielding of the detection areas with cooled copper plates. Figure 3 shows the structure around the collection area, which is marked by red. The shape of the collimation chamber was cut to be a pentagon so that this chamber would not cross the collection area. The thick solid lines indicate the cooled graphite-coated copper plates. This graphite coating is effective in suppressing the reflection of light emission from the chamber wall. The copper plates inside the emission collector chamber are connected to a Dewar with cooling reagents. The choice of either liquid $N_2$ or dry ice depends on the kind of measurement. In addition, a graphite-coated copper cylinder is inserted to shield the emission light path from the $CaF_2$ window to the FTIR spectrometer and connected to the second Dewar, which is usually filled with dry ice. The $CaF_2$ lens is also cooled by the third Dewar filled with ice. The spherical mirror is tilted on the copper plates and affixed by Ag paste so that the emission from the FTIR spectrometer cannot be detected. The shape of the copper plates was designed so that the $CO_2$ beam could not hit them. However, a small amount of scattered $CO_2$ still penetrated from the collimation chamber and was deposited on the cooled copper plates, yielding a significant pressure inside the emission collector. Thus, the emission from this $CO_2$ gradually became significant during the long-time signal accumulation when the copper plates had a closed shape. Therefore, it is also necessary to open the right side of the copper plates, as shown in Fig. 4, to pump out the scattered

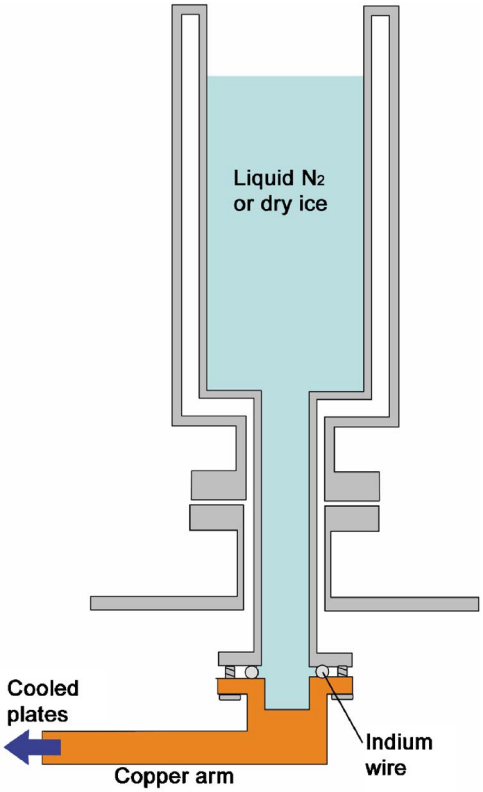


FIG. 5. (Color online) Dewar structure. The Dewar, which is made of stainless steel, is connected to the copper arm through an indium wire sealing. The bottom of the Dewar is open so that the copper arm makes direct contact with the cooling reagents.

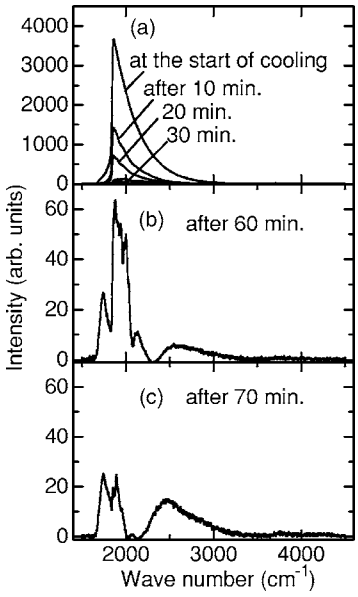


FIG. 6. FTIR emission spectra observed in the course of copper plate cooling. Each spectrum was obtained by 100 scans of the interferometer. The recording took about 1 min. (a) Spectra were recorded every 10 min in the course of the first 60 min of cooling, showing quick decreases. Typical spectrum after (b) 60 and (c) 70 min of cooling. The observed background emission intensity was mostly suppressed after 60 min.

$CO_2$.

Figure 4 shows a more realistic illustration of the copper plates inside the emission collector chamber. Although these plates consist of various parts, all parts are soldered together by a copper alloy to obtain better thermal conductivities. The copper plates are directly contacted with liquid $N_2$ or dry ice in the Dewar, as shown in Fig. 5. An indium wire (1 mm diameter) is used for sealing between the Dewar and the copper arm. The oxidation of the copper surface that contacts with liquid $N_2$ or dry ice at the top of the container reduces the cooling efficiency of the copper plates, seriously increasing the signals of the background emission in the FTIR spectra. Therefore, it is necessary to flow dry $N_2$ gas inside the container during apparatus baking to avoid the oxidation. In fact, the contact surfaces must sometimes be polished to remove the oxides.

## IV. TRIAL MEASUREMENTS

Figure 6 shows FTIR spectra obtained in the course of cooling of the copper plates. The background emission is seen only above 1800 $cm^{-1}$, since an InSb detector was used. The background emission mostly disappeared after 1 h of cooling, as shown in Fig. 6(a). Figures 6(b) and 6(c) show details of the spectra recorded 60 and 70 min after the start of cooling. The intensities below 2000 $cm^{-1}$ continued to decrease, whereas the signal above 2000 $cm^{-1}$ became noticeable after cooling. This signal increase is due to the contribution of the emission from some parts of the FTIR spectrometer itself. Since the phase response of this emission is different from that of emission from the copper plates, the interferograms of these two emissions cancel each other out. Therefore, the intensity in the spectrum decreases as the copper plates are cooled and then increases after the emission

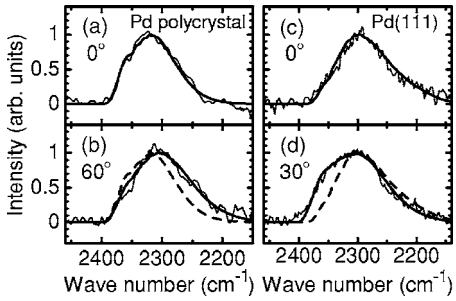


FIG. 7. Infrared emission spectra from the product $CO_2$ in CO oxidation on [(a) and (b)] well-annealed Pd polycrystalline foil and [(c) and (d)] Pd(111). The desorption angle of $CO_2$ is (a) 0° (the surface normal) and (b) 60° off normal and (c) 0° and (d) 30° off normal. The total exposure of CO and $O_2$ was fixed at $4.5\times10^{17}$ molecules/$cm^2$ s, yielding a pressure of $3.7\times10^{-3}$ Torr. The $CO/O_2$ ratio is 2:1, and the surface temperature is 700 K. The angle resolution is 16°. Fine lines show the observed spectra with a wave number resolution of 4 $cm^{-1}$. Thick solid lines show the optimum simulated results. These were obtained with (a) $T_{vib}=1300$ K and $T_{rot}=600$ K at 0°, (b) $T_{vib}=1700$ K and $T_{rot}=800$ K at 60°, (c) $T_{vib}=2100$ K and $T_{rot}=350$ K at 0°, and (d) $T_{vib}=1550$ K and $T_{rot}=1100$ K at 30°. For comparison, the best fits at 0° are drawn by the broken lines in (b) and (d).

from the FTIR spectrometer overcomes that from the copper plates. Thus, in order to accurately subtract the background, the phase response of radiation emitted from different positions was considered, i.e., the emission intensity was treated as complex numbers.[39]

Figures 7(a) and 7(b) show chemiluminescence spectra from the product $CO_2$ in CO oxidation on a well-polished Pd polycrystalline sample at different desorption angles. These were obtained as the difference between spectra recorded with and without the flow of reactant gases at a surface temperature of 700 K. In the process of subtraction, the emission intensities are treated as complex numbers. In each spectrum, a single broad peak appears in a range from 2400 to 2200 $cm^{-1}$, which consists of the contributions from a large number of transition lines corresponding to various initial rovibrational states. According to the previous measurements,[6–12] the populations of the vibrational and rotational states of product $CO_2$ are well expressed by the rotational and vibrational temperatures, $T_{rot}$ and $T_{vib}$, in the frame of the Boltzmann distributions. For the present low-resolution spectra, the position of the broad peak shifts toward lower wave numbers as $T_{vib}$ increases. On the other hand, the broad peak becomes wider when $T_{rot}$ is higher. The observed peak position in the spectrum at 0° appears at a higher wave number than that at 60°. This indicates that $T_{vib}$ at 0° is lower than that at 60°. In addition, the width of the peak at 60° is larger than that at 0°, indicating that $T_{rot}$ at 60° is higher than that at 0°.

The values of $T_{rot}$ and $T_{vib}$ can be estimated by the curve fitting of observed spectra with simulated ones.[8] In the simulation, the line positions presented in the Hitran database were used.[40] In addition, these line positions were linearly extended for transitions from higher rovibrational states. In the simulation, 1487 vibrational bands, each of which contains transitions from initial rotational states from $J=0$ to $J=270$, were used. In this case, simulated spectra cover about 98% and 95% of the total emission intensities at

$T_{vib}$=2000 K and $T_{vib}$=2500 K, respectively. The other transitions omitted in the simulation should yield smooth tails below 2200 $cm^{-1}$ outside the main peak. Neglecting these tails should hardly affect the estimation of $T_{rot}$ and $T_{vib}$. The contribution from each vibrational state for the symmetric, bending, and antisymmetric stretch modes could not be distinguished in this simulation, but $T_{vib}$ averaged over the three modes and $T_{rot}$ could be determined. Thick solid lines in Figs. 7(a) and 7(b) show the simulated results with the optimum values for $T_{rot}$ and $T_{vib}$, $T_{vib}$=1300 K (0°), $T_{rot}$=600 K (0°), $T_{vib}$=1700 K (60°), and $T_{rot}$=800 K (60°). For comparison, the simulated results for $T_{vib}$=1300 K and $T_{rot}$=600 K are also shown in Fig. 7(b) as the broken line, showing remarkable differences from the experimental result at 60°. The results on Pd(111) are quite different from those on the polycrystalline sample, as shown in Figs. 7(c) and 7(d), indicating that the internal energy is sensitive to the surface structure. The desorption-angle dependence is more remarkable on Pd(111), i.e., the estimated values are $T_{vib}$=2100 K (0°), $T_{rot}$=350 K (0°), $T_{vib}$=1550 K (30°), and $T_{rot}$=1100 K (30°). With an increasing desorption angle, $T_{vib}$ decreases, while $T_{rot}$ increases more quickly.

These remarkable differences in $T_{vib}$ and $T_{rot}$ at different desorption angles and crystal planes indicate that the measurements of the chemiluminescence from AR product $CO_2$ were successfully performed in the course of the catalyzed CO oxidation on flat palladium surfaces in the present apparatus.

## V. DISCUSSIONS AND REMARKS

Catalytic CO oxidation is one of the prototype reactions in surface chemistry that has led to new concepts in understanding surface reactions as well as contributed to the development of new advanced surface sensitive tools. In fact, in this reaction, the product desorption dynamics was first shown to be sensitive to the structure of product formation sites in thermal reactions.[41] The relation of desorption dynamics to the site structure will be elaborated by adding the desorption-angle dependence of the internal energies. This dependence indicates facile energy partitionings into the rotational, vibrational, and translational modes in different ways in a repulsive product desorption event.[4,34,41,42]

AR product desorption will deliver more information when it can be performed at a level of state-selective product analysis in the course of catalyzed reactions. This next stage becomes important in improving the method because each energy state of desorbing products will show different surface structures. This state resolved desorption dynamics will provide the most direct site-identification method applicable in the course of catalyzed reactions.

## ACKNOWLEDGMENTS

The authors thank Kazuhiko Matsudaira and Shingo Mukai at the CRC machine shop for their technical assistance in preparing each part of the apparatus. This work is partially supported by Grant-in-Aid No. 17350002 for General Scientific Research from the Japan Society for the Promotion of Science and also by the 1996 COE special equipment program of the Ministry of Education, Sports, and Culture of Japan.

[1] R. D. Levine and R. B. Bernstein, *Molecular Reaction Dynamics* (Oxford University Press, New York, 1974).
[2] H. Kasai and A. Okiji, Prog. Surf. Sci. **44**, 101 (1993).
[3] A. Hodgson, Prog. Surf. Sci. **63**, 1 (2000).
[4] T. Matsushima, Surf. Sci. Rep. **22**, 127 (1995).
[5] E. J. Heiweil, M. P. Casassa, R. R. Cavanagh, and J. T. Stephensen, Annu. Rev. Phys. Chem. **40**, 143 (1989).
[6] D. A. Mantell, S. B. Pyali, B. L. Halpern, G. L. Haller, and J. B. Fenn, Chem. Phys. Lett. **81**, 185 (1981).
[7] S. L. Bernasek and S. R. Leone, Chem. Phys. Lett. **84**, 401 (1981).
[8] D. A. Mantell, K. Kunimori, S. B. Ryali, G. L. Haller, and J. B. Fenn, Surf. Sci. **172**, 281 (1986).
[9] G. W. Coulston and G. L. Haller, J. Chem. Phys. **95**, 6932 (1991).
[10] H. Uetsuka, K. Watanabe, H. Ohnuma, and K. Kunimori, Surf. Sci. **377–379**, 765 (1997).
[11] K. Nakao, S.-I. Ito, K. Tomishige, and K. Kunimori, J. Phys. Chem. **109**, 17553 (2005).
[12] D. J. Bald and S. L. Bernasek, J. Chem. Phys. **109**, 746 (1998).
[13] H. A. Michelsen, C. T. Rettner, and D. J. Auerbach, Phys. Rev. Lett. **69**, 2678 (1992).
[14] C. T. Rettner and D. J. Auerbach, Phys. Rev. Lett. **74**, 4551 (1995).
[15] G. Comsa, R. David, and B. J. Schumacher, Surf. Sci. **95**, L210 (1980).
[16] H. Zacharias and R. David, Chem. Phys. Lett. **115**, 205 (1985).
[17] G. D. Kubiak, G. O. Sitz, and R. N. Zare, J. Chem. Phys. **83**, 2538 (1985).
[18] R. N. Carter, M. J. Murphy, and A. Hodgson, Surf. Sci. **387**, 102 (1997).
[19] M. J. Murphy, J. F. Skelly, and A. Hodgson, J. Chem. Phys. **109**, 3619 (1998).
[20] M. J. Murhy, J. F. Skelly, A. Hodgson, and B. Hammer, J. Chem. Phys. **110**, 8954 (1999).
[21] R. P. Thorman and S. L. Bernasek, J. Chem. Phys. **74**, 6498 (1981).
[22] R. P. Thorman and S. L. Bernasek, Rev. Sci. Instrum. **52**, 553 (1981).
[23] T. Matsushima, J. Chem. Phys. **91**, 5722 (1989).
[24] T. Matsushima, J. Chem. Phys. **93**, 1464 (1990).
[25] T. Yamanaka, C. Moise, and T. Matsushima, J. Chem. Phys. **107**, 8138 (1997).
[26] G. Cao, Md. G. Moula, Y. Ohno, and T. Matsushima, J. Phys. Chem. B **103**, 3235 (1999).
[27] M. Boudart, Adv. Catal. **20**, 153 (1969).
[28] M. Wilde, K. Fukutani, Y. Murata, M. Kampling, K. Al-Shamery, and H. J. Freund, Surf. Sci. **427–428**, 27 (1999).
[29] A. R. Burns, E. B. Stechei, and D. R. Jennison, Surf. Sci. **280**, 359 (1993).
[30] R. Schwalzwald, A. Modl, and T. J. Chuang, Surf. Sci. **242**, 437 (1991).
[31] J. Ahner, D. Mocuta, R. D. Ramsier, and J. T. Yates, Jr., Phys. Rev. Lett. **79**, 1889 (1997).
[32] T. Yamanaka, Y. Inoue, and T. Matsushima, J. Chem. Phys. **110**, 2597 (1999).
[33] M. Kobayashi and Y. Tuzi, J. Vac. Sci. Technol. **16**, 685 (1979).
[34] J. A. Barker and D. J. Auerbach, Surf. Sci. Rep. **4**, 1 (1985).
[35] T. Matsushima, Heterog. Chem. Rev. **2**, 51 (1995).
[36] J. Misewich, P. L. Houston, and R. P. Merrill, J. Chem. Phys. **82**, 1577 (1985).
[37] M. Wu, D. P. Taylor, and P. M. Johnson, J. Chem. Phys. **94**, 7596 (1991).
[38] W. H. Flygare, Acc. Chem. Res. **1**, 121 (1968).
[39] H. E. Revercomb, H. Buijs, H. B. Howell, D. D. LaPorte, W. L. Smith, and L. A. Sromovsky, Appl. Opt. **27**, 3210 (1988).
[40] L. S. Rothman, R. L. Hawkins, R. B. Wattson, and R. R. Gamache, J. Quant. Spectrosc. Radiat. Transf. **48**, 537 (1992).
[41] T. Matsushima, Chem. Phys. Lett. **155**, 313 (1989).
[42] G. Comsa and R. David, Surf. Sci. Rep. **5**, 145 (1985).